Computers and Geotechnics 176 (2024) 106789

Contents lists available at ScienceDirect

Computers and Geotechnics

journal homepage: www.elsevier.com/locate/compgeo

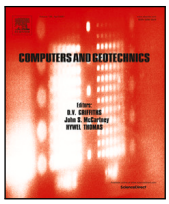

Research paper

Multiscale data-driven modeling of the thermomechanical behavior of granular media with thermal expansion effects

Rafael L. Rangel [a,b], Alessandro Franci [a,b,*], Eugenio Oñate [a,b], Juan M. Gimenez [a,c]

[a] Centre Internacional de Mètodes Numèrics a l'Enginyeria (CIMNE), 08034 Barcelona, Spain
[b] Universitat Politècnica de Catalunya (UPC BarcelonaTech), 08034 Barcelona, Spain
[c] Centro de Investigación de Métodos Computacionales (CIMEC), UNL/CONICET, 3000 Santa Fe, Argentina

ARTICLE INFO

Keywords:
Granular materials
Thermomechanical behavior
Thermal expansion
Continuum-discrete multiscale
Artificial neural network

ABSTRACT

A multiscale data-driven (MSDD) methodology is proposed for simulating the thermomechanical behavior of granular materials subjected to thermal expansion. The macroscale is handled using a continuous model based on the Finite Volume Method (FVM), while the microscale response is captured at Representative Volume Elements (RVEs) with the Discrete Element Method (DEM). To significantly reduce the computational cost of the analyses, the microscale DEM computations are not performed online, *i.e.*, simultaneously with the macroscale FVM ones, as generally done in standard multiscale approaches. Instead, they are performed in advance to create a comprehensive database of RVE solutions under different initial conditions and thermal strains. This dataset is then used to train an Artificial Neural Network (ANN), which serves as a surrogate model for the macroscale solver. The MSDD approach is validated against pure DEM solutions of problems with distinct thermal conditions. Remarkably, we demonstrate that with only three input parameters, namely porosity, fabric, and thermal strain, the surrogate model can predict the microstructure evolution, as well as the updated conductivity and Cauchy stress tensors of the granular assembly. This allows for a generally accurate simulation of transient thermomechanical analyses at a drastically lower computational cost than the pure DEM approach.

1. Introduction

Understanding the thermomechanical behavior of granular materials is of primary importance in several engineering problems. Packed beds of granular media are widely used as heat storage systems in renewable energy power plants (Ismail and Henrıquez, 2002). During heating-cooling cycles, thermal stresses due to differential expansion between the granular medium and the container can lead to potential material and structural damage (Sassine et al., 2018; Li et al., 2019). In the nuclear industry, packed beds of ceramic breeders are used for tritium fuel production in a fusion reactor. Under the effect of nuclear heating, the thermal expansion of breeders may lead to their breakage and an overall efficiency loss of the system. This explains the scientific interest in characterizing the thermomechanical behavior of ceramic breeder pebble beds (Reimann et al., 2002; Reimann and Hermsmeyer, 2002; Gan and Kamlah, 2007; Ying et al., 2012). Thermal expansion is also critical for asphalt concrete pavements (Chen et al., 2021), where cracking may be produced due to extreme temperature drops or fatigue induced by temperature fluctuations (Liu et al., 2021; Yin, 2015; Arabzadeh and Guler, 2019). On the other hand, as discussed in Chen et al. (2006) and Iliev et al. (2019), and studied numerically in Coulibaly et al. (2020), heating-cooling cycles of granular beds and the consequent thermal expansion–contraction may be conveniently used to compact the granular material without the need to apply external mechanical loads to the system. Remarkably, changes in packing fraction may affect the bulk properties of granular systems (Vargas and McCarthy, 2007), such as sound propagation (Liu and Nagel, 1994; Liu, 1994) and electrical conduction (Bonamy et al., 2000). In addition, thermal effects are also relevant in several manufacturing processes with granular materials, including, for example, granular mixing through rotating drums (Rangel et al., 2023) or bladed stirrers (Kisuka et al., 2023) and additive manufacturing via selective laser sintering (Kruth et al., 2003).

These are just a few examples highlighting the importance of modeling and predicting the thermomechanical behavior of granular media. However, this task proves highly challenging due to the intrinsic hybrid nature of granular matter, which possesses characteristics of both discrete and continuous materials and can behave simultaneously as a solid, fluid, and even as a gas (Herrmann and Luding, 1998; Campbell,

* Corresponding author at: Universitat Politècnica de Catalunya (UPC BarcelonaTech), 08034 Barcelona, Spain.
E-mail address: falessandro@cimne.upc.edu (A. Franci).

https://doi.org/10.1016/j.compgeo.2024.106789
Received 25 June 2024; Received in revised form 20 September 2024; Accepted 22 September 2024
Available online 26 September 2024

2006). Therefore, these properties make granular substances one of the most complex types of material to simulate.

Numerical methods offer the possibility to shed light on the complex nature of granular media. However, discrete strategies, such as the Discrete Element Method (DEM) (Cundall and Strack, 1979), while capable of faithfully representing the particulate nature of granular materials, may lead to unaffordable computational costs when applied to real-world problems. Continuous methods, such as the Finite Volume Method (FVM) (Versteeg and Malalasekera, 2007) or the Finite Element Method (FEM) (Zienkiewicz et al., 2005), have complementary characteristics, *i.e.*, they cannot capture the intrinsic behavior of granular media and require the use of phenomenological laws to model the material response, but they are applicable to real-scale simulations owing to their lower computational cost.

The dichotomy between continuous and discrete computational methods has led to the development of hierarchical multiscale approaches for the simulation of granular materials. In these hybrid strategies, a continuous method solves the macroscale problem deriving the material response from the homogenized solution of microscale analyses performed with a discrete method over Representative Volume Elements (RVEs) (Miehe and Dettmar, 2004; Miehe et al., 2010; Nguyen et al., 2014; Guo and Zhao, 2014; Liu et al., 2016). Typically, these approaches use the FEM for the macroscale solution and the DEM for the microscale analyses. More recently, particle-based methods, such as the Material Point Method (MPM) (Sulsky et al., 1994) and the Particle Finite Element Method (PFEM) (Idelsohn et al., 2004), have been employed as the macroscale continuous strategy to handle large material deformations (Liang and Zhao, 2019; Liang et al., 2021; Guo et al., 2021). All the mentioned multiscale formulations have focused solely on the mechanical behavior of granular media. Only recently have thermomechanical analyses been carried out with a hierarchical multiscale approach (Zhao et al., 2020, 2022; Yu et al., 2024).

Nevertheless, even for multiscale methods, the computational cost remains the bottleneck of the numerical approach. This is because the most computationally demanding procedure, *i.e.*, the DEM solution of granular assemblies, is performed at all integration points of the discretized continuous computational domain and in an online manner, *i.e.*, at each time step of the macroscale solution.

An attractive way to overcome this important limitation of hierarchical multiscale strategies is to perform the DEM microscale computations offline and use this information to train a surrogate model based on Machine Learning (ML) techniques, such as Artificial Neural Network (ANN). In the online macroscale computations, the surrogate model feeds the continuous solution with relevant information, such as stresses for a given deformation state (Wang and Sun, 2018, 2019a,b; Ma et al., 2022; Qu et al., 2023; Wang et al., 2024). In the context of thermal analysis of granular media, a multiscale methodology using an ANN-based surrogate model was presented in Desu et al. (2019) and Peeketi et al. (2019) to predict the effective thermal conductivity of a granular bed in a gaseous environment. An alternative method, yet still based on an offline–online multiscale approach, was recently proposed by the authors in Rangel et al. (2024) to estimate the temperature evolution in dense granular assemblies. A notable aspect of that work is the surrogate model's ability to accurately predict scale-invariant conductivities using only two dimensionless inputs that characterize the microstructure. Leveraging insights from the multiscale framework for turbulent flow simulations developed by the same research group (Gimenez et al., 2021; Idelsohn et al., 2024), the cited approach minimizes the number of parameters required for the offline database while broadening the applicability range of the methodology.

We also remark that ML-based algorithms trained with experimental measurements have been widely used to predict the effective thermal conductivity of materials with difficult characterization (Chen et al., 2024), such as composites (Wei et al., 2018), food (Sablani et al., 2002; Chayjan et al., 2007), textiles (Fayala et al., 2008), and rocks (Goutorbe et al., 2006; Singh et al., 2007), as well as in the context of granular media (Grabarczyk and Furmański, 2013; Go et al., 2016; Rizvi et al., 2020; Fei et al., 2021; Li et al., 2022; Zhang et al., 2020). However, creating an exhaustive database from experimental observations can be significantly more complex than from numerical results. Indeed, when training ML models with solely laboratory data, the limited amount and narrow scope of these data may restrict the applicability of the model and elevate the risk of extrapolation in its predictions.

In this work, we present a Multiscale Data-Driven (MSDD) methodology, based on the continuum-discrete hierarchical approach, for modeling the thermomechanical behavior of granular materials. Compared to our previous work (Rangel et al., 2024), which focused on heat conduction over a static medium, the new method is designed to address the transient behavior of granular media in the presence of thermal expansion. A dataset generated from offline DEM computations on RVEs of granular assemblies is created to train an ANN tool. The ANN works as a surrogate constitutive model for the macroscale solution framework, which is based on a volume-averaged FVM formulation. In this sense, for a given state of microstructural properties and thermal strain, the ANN forecasts the evolution of these properties, represented by porosity and fabric, as well as the updated conductivity and stress. A key benefit is that the evolution of microstructural properties is tracked based only on the initial configuration, without the need to simulate RVEs online. Furthermore, to the best of the authors' knowledge, this is the first application of an offline–online multiscale methodology to investigate the thermal expansion phenomenon in granular material. Remarkably, despite not solving the mechanical problem at the macroscale, the proposed MSDD approach is capable of predicting not only the time evolution of microstructural properties relevant for the thermal behavior, but also the evolution of local stresses without any significant additional computational cost.

To limit the complexity of the problem we assume some simplifying hypotheses. Firstly, we only focus on two-dimensional (2D) analyses of dense and dry granular matter. Furthermore, we consider particles with the same shape (circular) and material properties, and we also neglect the influences of gravity, shear effects, and interstitial air. Additionally, heat transfer takes place only by heat conduction through contact areas.

The remainder of the paper is structured as follows. Section 2 describes the proposed methodology. Firstly, it presents the formulations of the continuous and discrete methods used at the macro and micro scales, respectively, as well as the homogenization to link these two scales. Afterward, it describes the procedure for generating the database of microscale results and how it is used to train the ML-based surrogate model adopted. The section ends with the implementation algorithm for the online macroscale solution. Section 3 presents the results and discussions on the application of the method. Initially, it deals with offline procedures by showing features of the created database, as well as the ANN training process. Then it validates the online solution by comparing the results provided by the MSDD approach with a pure discrete solution. The section ends with a discussion of the limitations of the method. Finally, Section 4 gives concluding remarks and points towards future developments.

2. Methodology

An overview is provided for the multiscale data-driven (MSDD) methodology to solve the transient thermomechanical behavior of granular media considering heat conduction and thermal expansion. As shown in the schematic diagram of Fig. 1, the MSDD approach consists of two distinct, but communicating, frameworks: an *online* continuous computational method responsible for the *macroscale* solution, and an *offline* discrete strategy used to characterize the evolution of the *microscale* properties.

In the online procedure, the macroscale heat transfer problem is solved considering, at each integration point, effective microstructural properties inferred via a Machine-Learning (ML) surrogate model, which is implemented as an Artificial Neural Network (ANN). At a

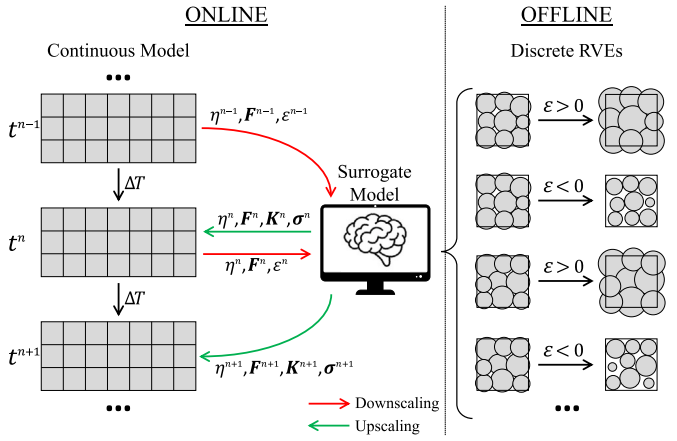

Fig. 1. General methodology scheme of the proposed MSDD approach.

given time step n of the online continuum computations, the current local porosity, η^n, fabric tensor, $\boldsymbol{F}^n$, and thermal strain, ϵ^n, feed the surrogate model that predicts the updated tensors of effective thermal conductivity, $\boldsymbol{K}^{n+1}$, Cauchy stress, $\boldsymbol{\sigma}^{n+1}$, and fabric, $\boldsymbol{F}^{n+1}$, as well as the updated local porosity, η^{n+1}.

In the offline procedure, the ML-based surrogate model is trained with data coming from discrete numerical analyses performed at the microscale over Representative Volume Elements (RVEs) of the granular material. The RVEs are simulated considering different initial consolidation conditions and applied thermal strains, which lead to expansion or contraction of the grains and, thus, new microstructure conditions. The porosity, fabric, and homogenized conductivity and stress tensors obtained at the equilibrium state before and after applying the thermal strains are stored in a database that is used to train the surrogate model.

2.1. Macroscale continuum formulation

At the macroscale, the time evolution of the temperature field T, within a domain Ω with boundaries Γ, is governed by the transient volume-averaged heat diffusion equation along with its associated boundary and initial conditions, expressed as:

$$\begin{aligned} \varrho c \frac{\partial T}{\partial t} &= \nabla \cdot (\boldsymbol{K} \nabla T) \quad \text{in} \quad [\Omega, t] \\ T &= \overline{T} \quad \text{in} \quad [\Gamma_{\mathrm{D}}, t] \\ \boldsymbol{K} \nabla T \cdot \boldsymbol{n}_{\Gamma} &= \overline{q} \quad \text{in} \quad [\Gamma_{\mathrm{N}}, t] \\ T &= T^0 \quad \text{in} \quad [\Omega, 0] \end{aligned} \tag{1}$$

where $\overline{T}$ is the imposed temperature on Dirichlet boundaries, Γ_{D}, $\overline{q}$ is the applied heat flux on Neumann boundaries, Γ_{N}, $\boldsymbol{n}_{\Gamma}$ is the outwards unit normal vector to the boundary, T^0 is the initial temperature field for the hyperbolic differential equation, and t denotes time.

Two effective properties describe the thermal behavior of the granular material: the conductivity tensor $\boldsymbol{K}$ and the volumetric heat capacity ϱc, being c the heat capacity of the grains and ϱ the bulk density. By neglecting the density of the interstitial air, we can assume that $\varrho = \rho(1-\eta)$, where ρ is the density of the particles and η is the porosity, defined as the local ratio of void to averaging volumes. We remark that these effective properties depend on the current microstructure, which can evolve due to thermal expansion. This intricate evolution cannot be captured by the continuous macroscale method and is modeled with discrete analyses performed at the microscale, as described in the next sections.

The solution of the transient diffusion problem in Eq. (1) can be obtained using standard numerical methods for the continuum. In this work, the spatial discretization is done via the cell-centered Finite Volume Method (FVM). Therefore, the domain Ω is split into non-overlapped volumes Ω_i, such that $\Omega = \bigcup_i \Omega_i$ and $0 = \bigcap_i \Omega_i$. A cell Ω_i is an arbitrary polyhedron whose boundary Γ_i is composed by flat faces b of normal $\boldsymbol{n}_b$ and area Γ_b, such that $\Gamma_i = \bigcup_b \Gamma_b$. The unknown field, T_i, as well as other necessary material properties, are stored in the cell center and linearly interpolated to the face mid-points when required. After spatial discretization and local balance procedures, the equation system is expressed as:

$$\sum_i \left((\varrho c)_i \left(\frac{\partial T}{\partial t} \right)_i \Omega_i - \sum_{b \in \Gamma_i} (\boldsymbol{K} \cdot \nabla T \cdot \mathbf{n})_b \, \Gamma_b \right) = 0 \tag{2}$$

The resulting system of algebraic equations is obtained from Eq. (2) once the time integration scheme and the spatial operators to approximate the fields and their derivatives at face mid-points are chosen. In particular, we employ an implicit first-order operator for the temporal term and second-order operators for the spatial approximations.

2.2. Microscale discrete formulation

The Discrete Element Method (DEM) is applied to simulate the granular behavior at the microscale. For simplicity, we focus only on two-dimensional (2D) problems, where single grains are represented as cylindrical particles of unit length, all moving within the same plane. As typically done in DEM approaches for thermal problems, all particles are assumed to be isothermal bodies. Furthermore, gravity and interactions with the air are not considered.

The translational motion, rotational motion, and temperature of each particle are solved by explicitly integrating the following equations:

$$m \frac{\mathrm{d}\boldsymbol{v}}{\mathrm{d}t} = \boldsymbol{f} \tag{3}$$

$$I \frac{\mathrm{d}\omega}{\mathrm{d}t} = M \tag{4}$$

$$mc \frac{\mathrm{d}T}{\mathrm{d}t} = q \tag{5}$$

where m, I, $\boldsymbol{v}$, ω, $\boldsymbol{f}$, M, and q are the mass, moment of inertia, translational velocity, angular velocity, resultant force, resultant torque, and net heat transfer of a particle, respectively. In this work, the resultant force acting on a particle is given by the sum of the contact forces with each neighbor, which are composed of normal and tangential components, $\boldsymbol{f}_n$ and $\boldsymbol{f}_t$, respectively, in addition to a non-viscous damping force, $\boldsymbol{f}_d$. The resultant torque arises from the sum of the contact torques with neighbors, M_c, which are provoked only by contact forces, as rolling friction is not considered. Finally, the net heat transfer of a particle is determined by the accumulation of heat conduction from/to each neighbor, q_c, which is calculated with a thermal pipe model. The models for calculating forces, torque, and heat transfer between elements are the same as those employed in our previous work (Rangel et al., 2024), whose formulas are summarized in Table 1.

The effects of thermal expansion are also considered. This phenomenon is modeled using a coefficient of linear thermal expansion, α. In this work, we assume that this material property is independent of temperature. Therefore, the increment in the radius of a particle over a time step, Δr, is calculated as:

$$\Delta r = \varepsilon r_0 \tag{6}$$

where the radial thermal strain, ε, is defined as:

$$\varepsilon = \alpha \Delta T \tag{7}$$

with ΔT being the temperature variation of the particle and r_0 its radius prior to the application of the temperature change. We note that mass conservation of individual particles implies that, if the volume of a particle changes due to thermal expansion, its density varies accordingly.

All computational implementations and simulations related to the microscale were done in the open-source framework *Kratos-Multiphysics* (Dadvand et al., 2010).

Table 1
DEM models for forces, torque, and heat transfer.

Contact normal force	$\boldsymbol{f}_n = -s_n \delta_n \boldsymbol{n}$
Contact tangential force	$\boldsymbol{f}_t = \begin{cases} \boldsymbol{f}_t^{\text{prev}} - s_t \Delta \boldsymbol{u}_t & \text{if } \lvert\boldsymbol{f}_t\rvert \le \lvert\boldsymbol{f}_n\rvert \tan(\varphi) \\ \lvert\boldsymbol{f}_n\rvert \tan(\varphi)\, \boldsymbol{t} & \text{otherwise} \end{cases}$
Particle damping force	$\boldsymbol{f}_d = -\mu \lvert\boldsymbol{f}_c\rvert \boldsymbol{v} / \lvert\boldsymbol{v}\rvert$
Contact torque	$M_c = \lvert\boldsymbol{f}_t \times \boldsymbol{l}\rvert$
Contact heat conduction	$q_c = -kA\,(T_1 - T_2) / \lvert\boldsymbol{d}\rvert$

Normal stiffness: $s_n = 2Er_1r_2/(r_1 + r_2)$. Tangential stiffness: $s_t = \nu s_n$. r_1, r_2, T_1, T_2: particles radii and temperatures. A: contact area. $\boldsymbol{d}$: branch vector between particles' centers. $\boldsymbol{n}$: unit outward normal of the contact. $\boldsymbol{t}$: unit vector in the contact tangential direction. δ_n: normal overlap. $\Delta \boldsymbol{u}_t$: increment of relative tangential displacement at the contact. E: Young's modulus. ν: tangential-to-normal stiffness ratio. φ: friction angle. μ: damping coefficient. k: thermal conductivity. $\boldsymbol{f}_c$: sum of contact forces with all neighbors. $\boldsymbol{f}_t^{\text{prev}}$: tangential force from previous time step. $\boldsymbol{l}$: lever arm of tangential force relative to particle's longitudinal axis.

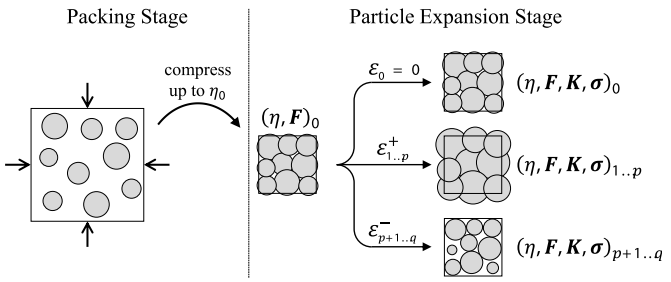

Fig. 2. Microscale data generation from a single RVE packing. The inputs of the database are the porosity and fabric after the packing stage and the applied thermal strains: $(\eta_0,\ \boldsymbol{F}_0,\ \varepsilon_i)$. The outputs of the database are the porosity and the tensors of fabric, conductivity, and stress after each strain application: $(\eta,\ \boldsymbol{F},\ \boldsymbol{K},\ \boldsymbol{\sigma})_i$. This two-step process is repeated for different RVE packings, *i.e.*, distinct $(\eta_0,\ \boldsymbol{F}_0)$.

2.3. Homogenization of the discrete behavior

The discrete solution of an assembly of particles must be represented by continuous-field variables to link the micro and macro scales. These variables are the porosity and the tensors of fabric, effective thermal conductivity, and effective stress. In this work, they are obtained exclusively from the particle positions and contact forces.

The fabric is computed following a popular contact-based tensorial definition (Oda, 1982), as:

$$\boldsymbol{F} = \frac{1}{N_c} \sum_{i=1}^{N_c} (\boldsymbol{n} \otimes \boldsymbol{n})_i \tag{8}$$

where N_c is the total number of contacts in the assembly and $\otimes$ denotes the outer product.

The effective thermal conductivity tensor is homogenized by considering only the geometry of the discrete solution and the thermal conductivity of the particles. For the thermal pipe model of heat conduction, this tensor is expressed as (Rangel et al., 2024):

$$\boldsymbol{K} = \frac{1}{V} \sum_{i=1}^{N_c} (kA\,\lvert\boldsymbol{d}\rvert\, \boldsymbol{n} \otimes \boldsymbol{n})_i \tag{9}$$

where V is the total volume of the considered assembly (area with unit depth in 2D). An advantage of this geometry-based approach for computing the effective thermal conductivity is that it does not require a thermal analysis of the granular material, as done in Desu et al. (2019) and Peeketi et al. (2019).

The force chain of the particle assembly is homogenized into the Cauchy stress tensor following the commonly used Love's formula (Christoffersen et al., 1981), as:

$$\boldsymbol{\sigma} = \frac{1}{V} \sum_{i=1}^{N_c} \left(\boldsymbol{d} \otimes (\boldsymbol{f}_n + \boldsymbol{f}_t)\right)_i \tag{10}$$

where the direction of the branch vector joining the particles' centers, $\boldsymbol{d}$, is such that compression is taken as positive. From the stress tensor, the mean effective stress, p, can be defined. In 2D, it is written as:

$$p = \frac{1}{2} tr(\boldsymbol{\sigma}) \tag{11}$$

2.4. Offline microscale simulations in RVEs

RVEs are employed to obtain information from the microscale and homogenize its discrete behavior. Following Rangel et al. (2024), the RVEs are square DEM assemblies with fixed, flat, and impenetrable walls as boundaries. In this type of mass-conserving RVEs, mass flow through the contours is not admitted, which implies that its bulk density and, consequently, the volumetric heat capacity can be assumed constant even if the volume of the particles changes.

The RVEs are composed of 500 particles; this number was shown to offer a good balance between the representativeness of the discrete medium and the computational cost for simulating RVEs with the mentioned conditions (Rangel et al., 2024). As explained in the cited study, the evaluation and homogenization of microstructural properties are carried out considering an internal region of the RVE, which is delimited by a convex hull formed by the center of all internal particles and some particles that touch the walls. A minor adjustment to this methodology was made in the present work, as it was observed that the previous one slightly underestimated the thermal conductivity. In this sense, the delimiting convex hull is formed only by internal particles that do not touch the walls, and all the contacts within or intersected by the boundary of this region are considered for evaluating Eqs. (8)–(10).

To generate the microscale dataset necessary to train the ML-based surrogate model, two stages of RVE simulations are performed offline: packing of granular assemblies and thermal expansion of particles. This two-step process is illustrated schematically in Fig. 2 for a single RVE packing.

The packing stage is the same as the RVE generation protocol described in Rangel et al. (2024). The boundaries move slowly to compact randomly positioned particles up to a target porosity. Different relative consolidation speeds in horizontal and vertical directions are used to control the principal direction of the fabric. The simulation ends when the particles reach static equilibrium after the walls stop moving. The resulting microstructure, with porosity η_0 and fabric tensor $\boldsymbol{F}_0$, is saved to allow the thermal expansion simulations to restart from it. Several RVE packing processes up to different target porosities are performed to generate the dataset.

In the thermal expansion stage, multiple simulations are performed for each RVE packing by applying different thermal strains, $\varepsilon_{0...q}$, to the particles. The thermal expansion effects are reproduced by changing the particle radii according to Eq. (6), meaning that strain values are prescribed without needing to change the temperature of the particles or solve a thermal problem in the RVEs. The thermal strain, either positive, ε^+, or negative, ε^-, is imposed uniformly on all particles in the RVE and at a slow rate to avoid excessive dynamic effects. During expansion, the boundaries are held still and friction with walls is considered. The simulation ends when the particles are in static equilibrium after reaching the target strain. At this moment, the new porosity and fabric tensor are evaluated, $(\eta, \boldsymbol{F})_{0...q}$, as well as the homogenized thermal conductivity and stress tensors, $(\boldsymbol{K}, \boldsymbol{\sigma})_{0...q}$.

2.5. Database of microscale results

Each thermal expansion simulation generates a data point of microscale results, consisting of input values that lead to an output solution. The initial configuration, represented by the initial porosity and fabric, together with the applied thermal strain, defines the inputs of the database, *i.e.*, $(\eta_0,\ \boldsymbol{F}_0,\ \varepsilon_i)$, while the final setup of the RVE determines the outputs, *i.e.*, $(\eta,\ \boldsymbol{F},\ \boldsymbol{K},\ \boldsymbol{\sigma})_i$. The scenario of zero strain, ε_0, is also contemplated by taking the initial and final configurations as

the same, thus without the need for an expansion simulation to create the data point.

The database must be created for input ranges sufficiently wide to cover the values that may occur in the intended problem. This is of primary importance to avoid extrapolation by the surrogate model, as it will be explained in the next section. Therefore, besides applying different thermal strains to the same RVE packing, several packing configurations are generated with varying porosities and fabrics as inputs. However, since the value of each input is varied independently of the others to cover the intended range, the number of RVE simulations required to create the database increases exponentially with the number of inputs. For this reason, it is crucial to reduce the database inputs as much as possible. Hence, as done in Rangel et al. (2024), we opt to disregard the off-diagonal, xy, components of the fabric tensor and, consequently, of the thermal conductivity and stress tensors. This decision is based on observing that, in the problems studied in this work, where no shear is imposed by the boundaries, the off-diagonal components of these tensors are much smaller in magnitude than their diagonal counterparts. In addition, since the trace of the fabric tensor is always equal to 1, its diagonal components can be represented by a single value in 2D. Therefore, we define a fabric index, f, given by $f = F_{xx} - F_{yy}$, which is taken as the sole parameter to represent the fabric.

We also observe that, due to the absence of gravity, the solution of square RVEs is frame invariant (Rangel et al., 2024). In 2D, this implies that we can generate additional data points through a 90° rotation of the tensorial variables of the original dataset. Therefore, each generated data point, with inputs $(\eta_0,\ f_0,\ \varepsilon_i)$ and outputs $(\eta,\ f,\ K_{xx},\ K_{yy},\ \sigma_{xx},\ \sigma_{yy})_i$, gives rise to a new data point whose inputs are $(\eta_0,\ -f_0,\ \varepsilon_i)$ and the outputs are $(\eta,\ -f,\ K_{yy},\ K_{xx},\ \sigma_{yy},\ \sigma_{xx})_i$, *i.e.*, the diagonal terms of tensors are swapped and, consequently, the sign of the fabric index changes.

To broaden the scope of the database and make it valid for granular materials with different properties, the inputs and outputs are stored in dimensionless form. The porosity, fabric, and strain already possess this characteristic. The thermal conductivity and stress tensors are normalized by adequate scaling factors into the dimensionless tensors $\widetilde{\boldsymbol{K}}$ and $\widetilde{\boldsymbol{\sigma}}$, respectively. The scaling factor of the effective thermal conductivity tensor is the conductivity of the particles used to create the database, hence: $\widetilde{\boldsymbol{K}} = \boldsymbol{K}/k$. This is because its homogenization formula (Eq. (9)) relies only on geometrical parameters, except for k, which is considered the same for all particles in this work. Therefore, normalization by particle conductivity makes the database independent of this property, as the homogenized thermal conductivity tensor can be rescaled accordingly. Analogously, the particle Young's modulus is taken as the scaling factor of the effective stress tensor, as it is the common parameter for calculating the contact forces in Eq. (10), hence: $\widetilde{\boldsymbol{\sigma}} = \boldsymbol{\sigma}/E$. This scaling operation allows the database to be reused for granular materials with different particle thermal conductivities and Young's moduli, provided that the dimensionless tensors are rescaled by the properties of the selected material. However, this is valid only for granular materials that share the same DEM modeling features as those used to create the database. These include contact and heat transfer formulations, particle shape and size distribution function, the use of a single material type, and general assumptions like neglecting gravity. Any change to these conditions would alter the microscale results of homogenized conductivity and stress tensors in ways that the scaling operation cannot account for. We also note that, regardless of non-dimensionalization, the database remains applicable to materials with varying densities, specific heat capacities, and thermal expansion coefficients, as these properties do not affect the microscale results under the assumptions of this work. Furthermore, although the function of particle size distribution must match to allow re-utilization of the database, the size magnitudes can be different.

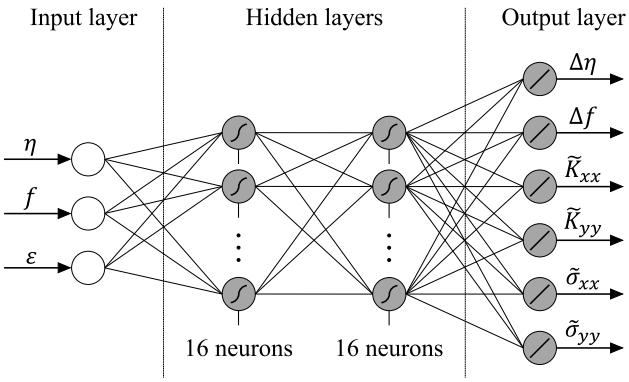

Fig. 3. Architecture of the adopted ANN.

2.6. Microscale surrogate model

An Artificial Neural Network (ANN) is used as a surrogate model to predict the microscale behavior based on the database of RVE solutions. Following Rangel et al. (2024), a feed-forward multilayer network is employed. The general ANN architecture has an input layer, a set of hidden layers, and an output layer. The first contains artificial neurons that receive the input values; in this case, the porosity, fabric index, and thermal strain. In each hidden and output layer, there are artificial neurons interconnected via adaptive weights. These weights are calibrated through a training process with the input–output values of the database. There is no general rule to define a proper ANN structure in terms of the number of hidden layers and artificial neurons. Therefore, the ANN architecture adopted in this work was calibrated by trial and error. As depicted in Fig. 3, it is formed by two hidden layers of 16 neurons, for which the tangent sigmoid is selected as the activation function. The output layer has 6 neurons, for which linear activation functions are used to provide the values of porosity and fabric index increments ($\Delta\eta$ and Δf), as well as the diagonal components of the dimensionless thermal conductivity and stress tensors ($\widetilde{K}_{xx}$, $\widetilde{K}_{yy}$, $\widetilde{\sigma}_{xx}$, $\widetilde{\sigma}_{yy}$). Moreover, to improve training convergence, the output values are normalized from 0 to 1.

It is worth mentioning that the thermal conductivity of a granular medium can be accurately obtained from its current state of porosity and fabric alone, as shown in Rangel et al. (2024). A similar conclusion is expected for the stresses, which could also be predicted directly from the instantaneous assembly configuration without information about thermal strain imposition. The thermal strain is mandatory only for the incremental outputs that dictate the evolution of the microstructure. This provides generality to the methodology by allowing the use of decoupled surrogate models. For instance, in the case of already disposing of a surrogate model relating porosity and fabric to conductivity and stress, one could focus on developing a more compact model to predict only the evolution of porosity and fabric resulting from thermal strains.

The ANN training performance is quantified with the coefficient of determination R-squared (R^2). It is calculated as:

$$R^2 = 1 - \frac{\sum_{i=1}^{N}(D_i - P_i)^2}{\sum_{i=1}^{N}(D_i - [D])^2} \tag{12}$$

where D_i and P_i are the computed (via DEM) and predicted (via ANN) values for the sample i, respectively, and the square brackets denote the mean value. A perfect agreement is obtained when R^2 is equal to one.

Furthermore, it is crucial to ensure a consistent evolution of porosity and fabric, particularly for the case of zero thermal strain when the increments of these properties must be null. Although the data points of zero strain are generated considering an unchanged configuration of porosity and fabric, the ANN prediction surface does not necessarily

pass exactly at these points. Therefore, we enforce this condition in the post-processing stage of the training results.

The validity of the ANN is guaranteed only for the range of input values covered during the training, as extrapolated results may not be reliable. Therefore, it is necessary to define the region of reliable ANN predictions within the hyper-space of input points. In this work, we propose building a convex hull over the three-dimensional cloud of input points. This region defines the range of porosity, fabric index, and thermal strain values within which the surrogate model is more likely to predict reliable outputs for a given problem.

2.7. Online macroscale algorithm

Algorithm 1 summarizes the tasks performed at each time step of the online macroscale solution to address the transient heat problem formulated in Eq. (2). The macroscale and microscale solutions are coupled by means of a first-order explicit time integration strategy that can be classified as Gauss–Seidel scheme.

The effective material properties required for the solution of the macroscale governing equation are the conductivity tensor and the volumetric heat capacity at each FVM cell. The former is obtained from the surrogate model, Φ, using the current local porosity, fabric index, and thermal strain as inputs. Concerning volumetric heat capacity, this property does not vary over time in the present context. This is because the local bulk density is constant as a consequence of the microscale modeling via mass-conserving RVEs. Instead, the particle density field may vary with time, and its local values can be estimated from the bulk density and the updated porosity, as shown in step 3.

We also point out that the thermal strain must be adjusted before consulting the surrogate model. This is because, in an RVE simulation, the strain is imposed relatively to the initial RVE configuration, which corresponds to the current configuration in the macroscale problem, *i.e.*, at time step n. However, to agree with the linear thermal expansion model, the strain should be relative to the macroscale initial configuration, *i.e.*, at time step $n = 0$. The consistency of thermal strain is achieved, after simple algebraic manipulation, by applying an adjustment factor β, as shown in step 5.

Additionally to the variables required for the solution of the governing equations, other relevant homogenized fields can be tracked locally at the macroscale level, such as the Cauchy stress. The results of stress evolution can be employed for post-processing, as it is an output of interest in various applications.

The computational implementation of this algorithm was carried out on the open-source platform OpenFOAM (Weller et al., 1998) via an in-house *solver*. This solver includes the coupling technology that enables feeding the continuous model, at each time step and FVM cell, with local material properties given by the surrogate model.

Algorithm 1 - Time step solution of the online continuous solver in the MSDD method.

Given the known fields at time step n: η^n, f^n, ε^n, ϱ^n, T^n; the fixed material properties k, E, and α; and the initial temperature T^0, do for each cell:

1. Query the surrogate model:

$$[\Delta\eta, \Delta f, \widetilde{\boldsymbol{K}}, \widetilde{\boldsymbol{\sigma}}] = \Phi(\eta^n, f^n, \varepsilon^n)$$

2. Update the effective material properties:

$$\eta^{n+1} = \eta^n + \Delta\eta$$
$$f^{n+1} = f^n + \Delta f$$
$$\boldsymbol{K}^{n+1} = k\widetilde{\boldsymbol{K}}$$
$$\boldsymbol{\sigma}^{n+1} = E\widetilde{\boldsymbol{\sigma}}$$

3. Update the bulk and particle densities:

$$\varrho^{n+1} = \varrho^n \qquad i.e., \text{ constant in this work}$$
$$\rho^{n+1} = \varrho^{n+1}/(1 - \eta^{n+1})$$

4. Solve Eq. Eq. (2) for the updated temperature T^{n+1}
5. Update and adjust the thermal strain:

$$\varepsilon^{n+1} = \alpha(T^{n+1} - T^n)\beta^{n+1} \qquad \text{with} \qquad \beta^{n+1} = \frac{1}{1 + \alpha(T^n - T^0)}$$

3. Results and discussion

In this section, the proposed methodology is validated for simulating the thermomechanical behavior of a granular medium subjected to temperature variations. In the offline computations, we generate the database of microscale results and train the ANN to predict the behavior of the given material. To validate the online macroscale computations, the results obtained with the proposed MSDD approach using the trained ANN are compared with those of a pure DEM model, which is taken as a reference discrete solution.

The properties of the granular material used in this investigation are indicated in Table 2. Those are fictitious parameter values intended solely for method validation. When informed, specifically in the analyses without thermal expansion, the coefficient α assumes a zero value. The particle size distribution follows the one used in Rangel et al. (2024) and is characterized by a constant function of the radius with mean, minimum, and maximum values of 5.0 mm, 3.0 mm and 7.0 mm, respectively.

Table 2
Properties of the granular material used to apply the proposed MSDD methodology.

Property	Value
Density, ρ [kg/m^3]	3000
Young's modulus, E [MPa]	10
Stiffness ratio, ν [–]	0.8
Friction angle, φ [–]	0.5
Thermal conductivity, k [W/(m·K)]	100
Specific heat capacity, c [J/(kg·K)]	1.0
Thermal expansion coefficient, α [–]	0.001
Damping coefficient, μ [–]	0.1

3.1. Offline computations and training analysis

3.1.1. Generation of the database of microscale results

The database of microscale results was created for a wide range of values of input porosity, fabric index, and thermal strain to allow its applicability for diverse conditions of the granular material. In total, 5172 data points were generated. Fig. 4 depicts these points as black dots in the three-dimensional input space. The filled volume represents the convex hull that defines the region of reliable ANN predictions of the outputs. This region should cover the input values that occur in the validation examples presented later in this work.

Through different RVE packing processes, we could cover a range of porosity from, approximately, 6.0% to 19.5%. It must be noted that the lower limit of porosity can only be reached in 2D DEM assemblies by permitting large, typically non-physical, overlaps between particles. This allows us to verify the validity of the proposed methodology under extreme thermal expansion conditions. The upper limit corresponds to the porosity around which the particle assemblies reach a loose packing state and the force chain is disrupted.

To vary the fabric at each porosity level, isotropic and horizontal compressions were performed, with the former leading to near zero fabric indexes and the latter resulting in greater positive fabrics indexes, *i.e.*, with dominant F_{xx} component. The data points with larger negative magnitudes of fabric index were generated through orthogonal rotation of the data obtained in the RVE simulations. Because of this, the distribution of data points in the $\eta \times f$ plane is symmetric with

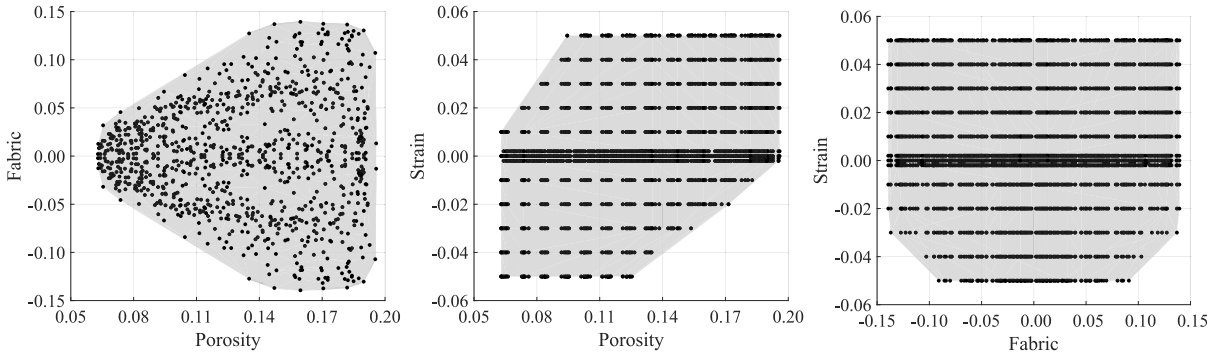

(a) Projection in plane $\eta \times f$. (b) Projection in plane $\eta \times \varepsilon$. (c) Projection in plane $f \times \varepsilon$.

Fig. 4. Data points in the input space and the valid ANN prediction region.

respect to $f = 0$, as seen in Fig. 4(a). Moreover, the maximum range that can be achieved for the fabric index is related to the porosity to which the assembly is compressed. In general, as also observed in Fig. 4(a), the lower the porosity, the narrower the fabric index range. This is because, in a dense packing, the particles come into contact with neighbors in more diverse directions, thus reducing the predominance of a principal fabric direction, *i.e.*, the values of F_{xx} and F_{yy} are closer to each other. On the other hand, in a more porous configuration, a greater proportion of existing contacts is related to the principal direction.

For each RVE packing condition, with a certain input value of porosity and fabric index, strains from −5% to 5% were applied during the expansion stage. These bounding values correspond to a temperature change of 50 K, which is the maximum possible temperature variation the particles can experience in the upcoming validation examples. However, the vast majority of time step increments of temperature that will be observed in the continuous macroscale model is much lower than that upper limit. In fact, most input thermal strains are expected to be minimal. Therefore, as evidenced in Figs. 4(b) and 4(c), a larger number of data points was generated for small strain values in order to ensure an optimal training of the ANN within this input region.

3.1.2. ANN training

The training of the ANN was accomplished with Matlab's deep learning toolbox. The dataset was randomly split into training, validation, and testing subsets, considering proportions of 70%, 15%, and 15%, respectively. For the training function, the Levenberg–Marquardt backpropagation algorithm was selected, considering a learning rate of 10^{-4} and the mean squared error (MSE) as the convergence indicator. Convergence was assumed when the MSE showed no improvement for 20 consecutive epochs, which occurred at epoch 92.

The fittings that compare the results of ANN-predicted and DEM-computed outputs, for all input points, are presented in the scatter plots of Fig. 5, where the dashed line represents the ideal fitting of $R^2 = 1$ according to Eq. (12). For the increment of porosity, the fitting is nearly perfect, with $R^2 = 0.999$. The increment of the fabric index, although still satisfactory, shows the worst training performance among the considered outputs, with $R^2 = 0.859$. This might be caused by the influence of other parameters not considered as inputs for predicting fabric variations. Furthermore, variations in the contact network are intrinsically subjected to the randomness of particle positions and movements in the assembly, making it very challenging to achieve high precision of its prediction using deterministic parameters. The components of the dimensionless thermal conductivity and stress tensors present similar coefficients of determination ($R^2 = 0.989$ and $R^2 = 0.980$, respectively), with the thermal conductivity showing a slightly better fitting than the stress.

Table 3
R^2 values of each output considering different sets of inputs in the ANN.

Inputs	$\Delta\eta$	Δf	$\widetilde{K}_{xx}$, $\widetilde{K}_{yy}$	$\widetilde{\sigma}_{xx}$, $\widetilde{\sigma}_{yy}$
η, f, ε	0.999	0.859	0.989	0.980
η, ε	0.998	0.003	0.935	0.851
f, ε	0.985	0.834	0.358	0.362
η, f	0.132	0.256	0.649	0.664

Overall, the obtained coefficients of determination are considered sufficiently accurate for the goals of this work. They indicate that variations in the outputs can be accurately explained by the chosen input parameters, thus justifying the selection of porosity, fabric, and thermal strain as inputs for the ANN. This also reveals that we are not missing any indispensable parameter as input to the surrogate model.

To evaluate the impact of individual inputs on the prediction of each output, alternative ANNs were implemented by removing one input at a time from the original network of Fig. 3. Table 3 gives the coefficients of determination of each output obtained with different sets of inputs; the first line replicates the results from the original set, while subsequent lines exclude one of the inputs. The more influential an input parameter is, the greater the degradation in training performance. It is interesting to observe that the thermal strain is the only essential parameter for the porosity increment, and that the porosity does not have a crucial effect on fabric variation, while the other inputs do, yet it is much more relevant than the fabric for predicting thermal conductivity and stress. However, the fabric has considerably more impact on stress than on conductivity. Furthermore, it can be concluded that there is no surplus of input parameters in our model, as each of them has a significant effect on one or more outputs.

Fig. 6 shows ANN output surfaces in cross-sections of the reliable prediction region. They reveal important features of the microscale behavior and confirm some of the discussed input effects. From Fig. 6(a), it is clear that the porosity increment varies only with the input strain, and the input fabric index has negligible effects. A resembling behavior occurs in the $\eta \times \varepsilon$ cross-sections (not shown for simplicity) but with a slightly greater influence of the input porosity. Fig. 6(b) proves that the increment of fabric index presents a reduced dependence on the input porosity. Furthermore, from this positive strain cross-section ($\varepsilon = 0.01$), it can be noted that positive inputs of the fabric index yield negative increments, while negative inputs result in positive increments. In other words, the absolute value of the fabric index decreases when the particles expand. A similar, but opposite, behavior occurs with negative strains (not shown), *i.e.*, the absolute value of fabric index tends to increase as the particles contract. This relates to the range of fabric index that could be achieved for different porosities in the previous section. As explained, in general, higher coordination numbers lead to

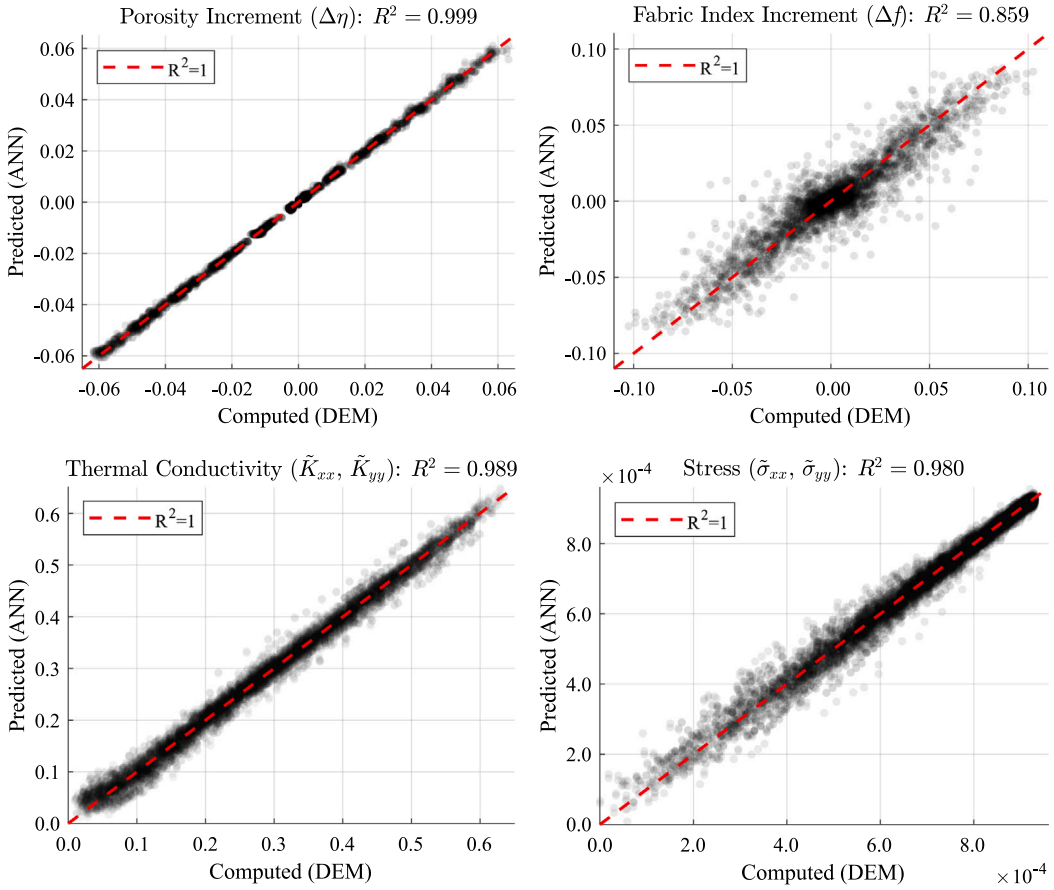

Fig. 5. Fitting of the ANN predictions against DEM results of each output.

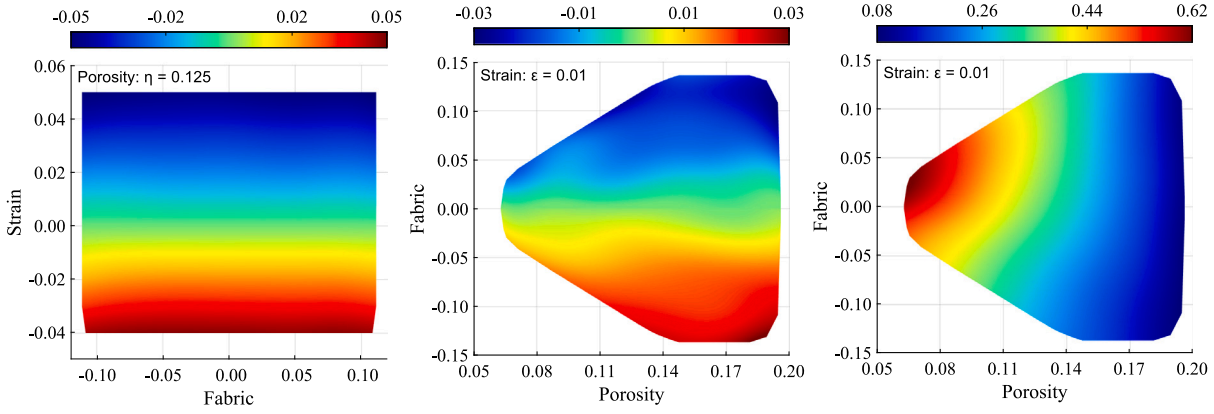

(a) Porosity increment ($\Delta\eta$). (b) Fabric increment (Δf). (c) Thermal conductivity ($\widetilde{K}_{xx}$).

Fig. 6. ANN output surfaces in cross-sections of the valid prediction region.

a more uniform distribution of contact directions. Fig. 6(c) shows the behavior of the xx component of the dimensionless conductivity tensor. Clearly, the thermal conductivity gradient is steeper towards input porosity than towards fabric, thus evidencing the greater relevance of the former. The yy component presents a mirrored pattern and a similar behavior is obtained for the stresses, therefore they are not shown.

These and other complex relationships between microstructural parameters were only possible to be captured due to the use of an ML tool. In particular, we were able to implement a compact surrogate model, with relatively few inputs, that can predict intricate features of the microscale behavior with good accuracy.

3.2. Online computations and results validation

3.2.1. Simulated models

The reference DEM model is shown in Fig. 7. It consists of a rectangular box 2150 mm wide and 645 mm high, with flat walls as boundaries and containing 15 000 particles. The thermomechanical material properties and particle size distribution are the same as before. However, due to the non-dimensionalization of the microscale database, a material with some different properties, such as Young's modulus, density, heat capacity, and thermal conductivity, could be used. The control points P1, P2, and P3 used to measure local temperatures are also indicated in Fig. 7. These points are positioned at

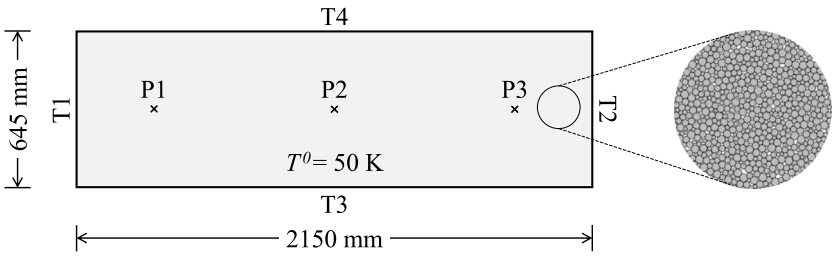

Fig. 7. Reference DEM model indicating the dimensions, the control points P1, P2, P3, and the thermal boundary conditions for the analysis cases provided in Table 4.

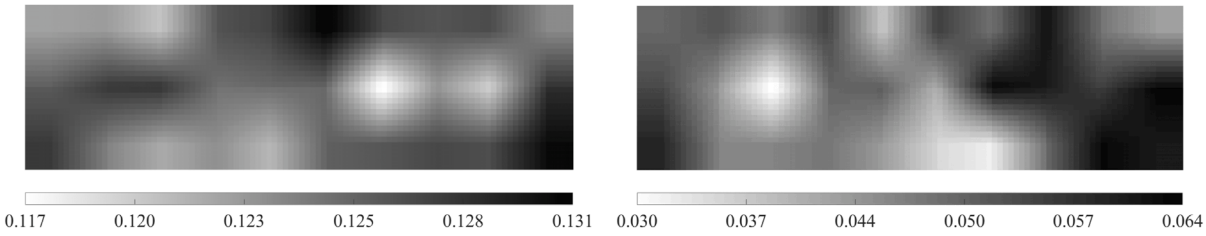

(a) Initial porosity (average = 0.125) (b) Initial fabric index (average = 0.050)

Fig. 8. Initial properties assigned to FVM cells as obtained from the reference DEM model.

the mid-height of the model, with P1 and P3 situated 322.5 mm from the lateral walls and P2 located at the center. In the DEM model, the temperature is taken from the closest particle to the control points.

Analysis cases with distinct thermal boundary conditions and expansion coefficients were simulated. These cases are indicated in Table 4. They consist of three thermal boundary conditions for the walls, named as hot (H), cold (C), and hot–cold (HC), each one being simulated with and without the consideration of thermal expansion. The initial temperature of the granular material is 50 K in all analysis cases. These cases were selected because they allow the exploration of different behaviors of the granular material provided by heating and cooling effects.

The same analysis cases were reproduced with the MSDD methodology. Therefore, an FVM model was created by discretizing the granular domain into a structured mesh of 100 × 30 square cells. The FVM cells were assigned the same material properties as the DEM particles for density, ρ, specific heat capacity, c, and thermal expansion coefficient, α. To apply the proposed MSDD method, it is necessary to determine the local porosity and fabric in the initial configuration. At each FVM cell, the porosity is employed to compute the bulk density, while the combination of both properties serves as input for the previously trained ANN to predict the initial thermal conductivity and stress tensors. In this work, the FVM cell values of porosity and fabric index are obtained from the reference DEM model. They are computed considering a 215 mm square region, which contains an average of 500 particles, around each cell. Fig. 8 shows the color maps of initial porosity and fabric index obtained for the FVM cells. The porosity ranges from 11.7% to 13.1%, averaging 12.5%, while the fabric index spans 0.030 to 0.064, with an average of 0.050. We remark that, in practice, when a DEM model of the material is not available, these local microstructural properties could be acquired through other means, such as experimental methods (Yang et al., 2008; Vlahinić et al., 2014; Wiebicke et al., 2020) or appropriate assumptions of their values.

The total analysis time was set to 20 s in all cases. A time step size of 5×10^{-5} s was used in the DEM simulations, while 10^{-3} s was employed for the FVM. These values were determined through sensitivity analyses, such that further reductions in the time step size produce negligible variations in the results (a convergence analysis of the MSDD results is presented in Section 3.2.4). Remarkably, the average wall-clock time for DEM and FVM simulations, on a personal computer with standard configurations, was around 30 h and 40 s, respectively. Therefore, the proposed MSDD methodology presented a speedup factor in the order of 3×10^3 compared to the discrete method.

Table 4
Thermal properties and boundary conditions for different analysis cases of the model in Fig. 7.

Case ID	α [/K]	T1 [K]	T2 [K]	T3 [K]	T4 [K]
H*	0	100	100	100	100
H	0.001	100	100	100	100
C*	0	0	0	0	0
C	0.001	0	0	0	0
HC*	0	100	0	Insulated	Insulated
HC	0.001	100	0	Insulated	Insulated

The accuracy of the results obtained with the MSDD approach is analyzed in the next sections. This will be done by comparing the spatial distribution and time evolution of microstructural properties and temperature against the reference DEM model. The discrete results of microstructural properties, such as the homogenized tensors of fabric, thermal conductivity, and Cauchy stress, are computed via Eqs. (8)–(10) in the DEM model. To apply these homogenizing equations, a sufficiently large assembly of particles needs to be considered. Therefore, in order to compare the spatial distribution of microstructural properties between the discrete and continuous models, the DEM domain is subdivided into a grid of 10 × 3 square sub-regions for homogenizing its results in each of them. This grid was chosen because its sub-regions contain 500 particles on average, the same number of particles as the RVEs used in this work, which was determined to provide a good representation of the discrete behavior (Rangel et al., 2024). The same grid is also used to subdivide the FVM mesh and post-process the MSDD results. In this case, each sub-region contains 10 × 10 FVM cells, and the reported result value in a sub-region corresponds to the mean value of its 100 cells. This post-processing is to allow a fair comparison of the results in the continuous model with the DEM, so that the values are averaged over the same regions.

3.2.2. Analyses without thermal expansion

Initially, the analysis cases without thermal expansion are briefly examined (cases H*, C*, and HC*). In these purely thermal problems, the

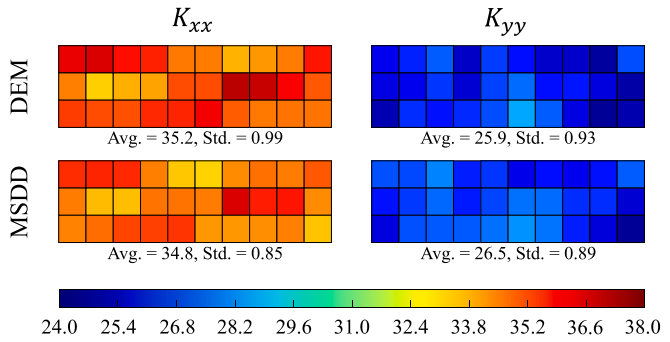

Fig. 9. Comparisons of the initial values of the thermal conductivity tensor components. The average (Avg) and standard deviation (Std) of the sub-region values are indicated. All units are in W/m·K.

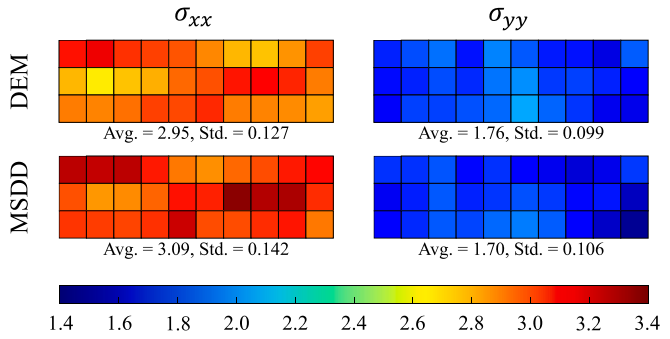

Fig. 10. Comparisons of the initial values of the Cauchy stress tensor components. The average (Avg) and standard deviation (Std) of the sub-region values are indicated. All units are in kPa.

microstructure remains unchanged throughout simulations. Therefore, the ANN is consulted by the continuous model only at the beginning of the simulation to estimate the local conductivity and stress of each FVM cell from the initial porosities and fabric indexes shown in Fig. 8. This is the same problem type tackled in our previous investigation (Rangel et al., 2024) and it shows the ability of the methodology to estimate the conductivity and stress tensors for a given state of porosity and fabric.

Fig. 9 shows color maps comparing the xx and yy components of the thermal conductivity tensors obtained in the reference DEM model and predicted by the ANN in the MSDD approach after being scaled by the particles' conductivity. A similar comparison is presented for the Cauchy stress tensor components in Fig. 10, in this case by scaling the predicted stress by the Young's modulus of the particles. In both cases, the MSDD results present excellent agreement with the DEM results. The greatest error of the average values, relative to the reference solution, is 5%, which is observed in the xx components of the stress tensor. Indeed, a larger error was expected for stress than for conductivity, as the ANN fitting was slightly less precise for the former. The temperature evolution at the center (point P2) of the DEM and FVM models is compared for each analysis case in the graph of Fig. 11. Again, an excellent agreement was achieved.

3.2.3. Analyses with thermal expansion

When thermal expansion is considered (cases H, C, and HC), changes in particle size cause the microstructural properties to evolve over time. Particularly in our methodology, the evolution of these properties is dictated by the porosity, fabric, and thermal strain, which are passed as inputs of the ML-based surrogate model. As previously discussed, it is important for the input values to remain inside the valid ANN prediction region, so the outputs can be considered reliable. Fig. 12 depicts all the input points, projected onto the porosity-fabric plane, that the FVM cells use to consult the ANN throughout the

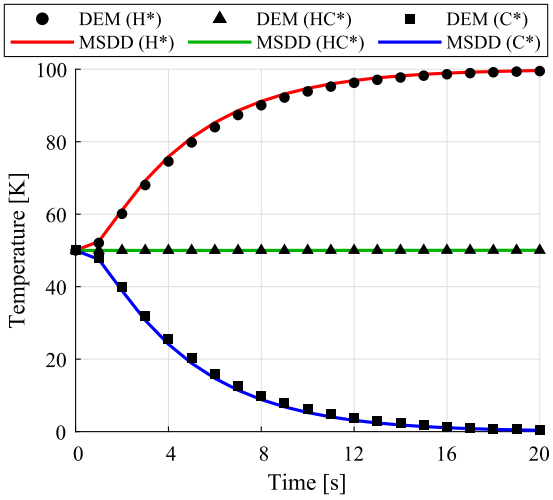

Fig. 11. Temperature evolution at the central point (P2): analysis cases without thermal expansion.

simulation of each analysis case. The color scale indicates the time when the values are reached and the gray area represents the region we defined as valid due to the low probability of extrapolation. In case H, the porosity and fabric index decrease from the initial configuration, reaching the final configuration relatively quickly. In case C, both properties increase in value, but the evolution occurs at a slower pace. Case HC covers the spectrum of porosity and fabric exhibited by the previous cases. In all cases, the input points stay within the valid region. Although not shown, the thermal strain values, which are very small in most solution steps, also remain inside the defined region. Therefore, aggressive extrapolations are ensured not to happen during the prediction of outputs in any analysis case.

The porosity represents an important result for granular materials, not only for their thermal behavior, but for characterizing different microstructure properties, such as permeability. To provide a visual representation of the porosity variation across the analysis cases, Fig. 13 shows the final configuration around the center of the reference DEM model, with the average porosity of the cropped regions indicated. Fig. 14 provides color maps comparing the final porosities obtained in the DEM model with the solutions from the MSDD approach, for each analysis case. The MSDD results show very good agreement with the DEM, with slight underestimations of the final porosity variation in the analysis cases H and C. In case HC, the results are also very similar across much of the domain, but with a concentrated overestimation of porosity by the MSDD solution near the cold wall.

A potential cause for the porosity difference on the cold side of case HC is the bulk motion of particles within the granular medium due to thermal expansion. As particles expand and contract in different zones of the domain, the porosity gradient triggers a mass flux between zones of higher and lower bulk density. This is evidenced in Fig. 15, which displays the magnitude of horizontal displacement of DEM particles at the end of the analysis. Notably, the most intense motion occurs on the cooled side, where the MSDD approach struggles more. We remark that this motion is also seen in the analysis cases H and C, but with much less intensity, as the porosity gradients are minimal. This macroscale phenomenon, whose impact is also noted in the subsequent results, is a limitation of the MSDD methodology. This is because multiscale hierarchical approaches cannot capture these effects at the microscale with mass-conserving RVEs.

Fig. 16 shows color maps comparing the xx and yy components of the thermal conductivity tensors obtained in the reference DEM model and with the MSDD approach at the end of each analysis case. In general, they reflect the accurate results obtained for the porosity, as

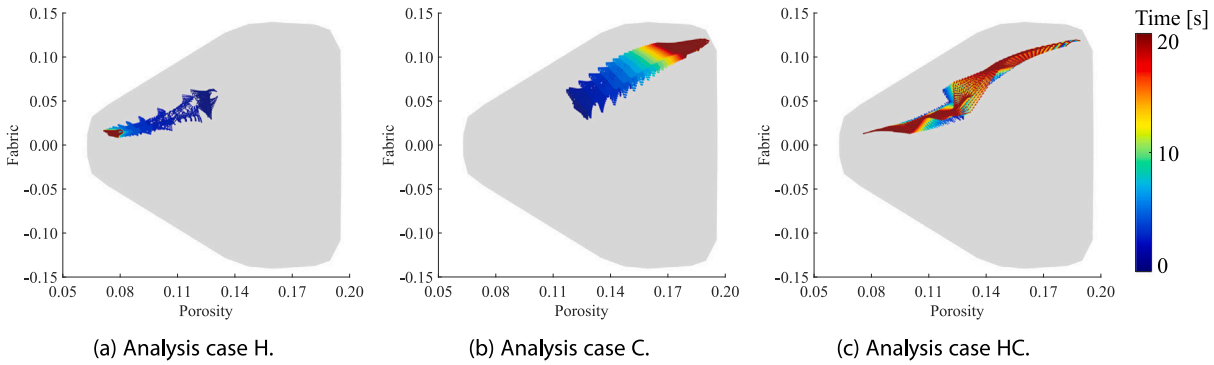

Fig. 12. Evolution of input values of FVM cells in each analysis case projected onto the $\eta \times f$ plane.

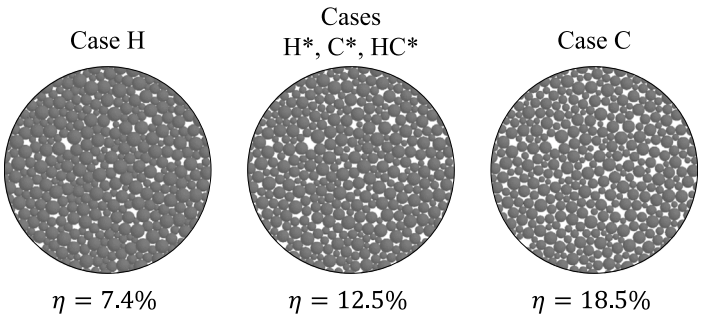

Fig. 13. Final microstructure around the center (point P2) of the reference DEM model in different analysis cases. The average porosity in the cropped regions is indicated.

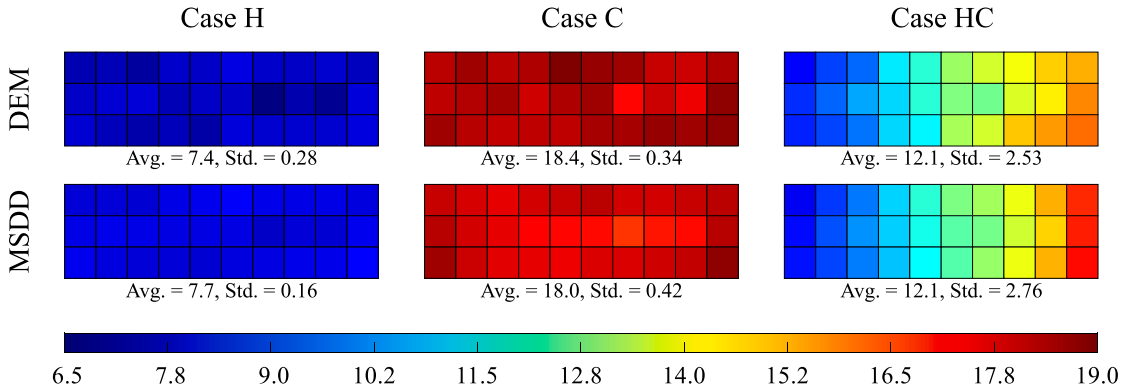

Fig. 14. Comparisons of the final values of porosity. The average (Avg) and standard deviation (Std) of the sub-region values are indicated. All values are given in percentage (%).

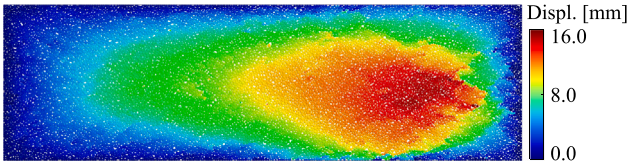

Fig. 15. Final horizontal displacement of DEM particles in the analysis case HC.

it has been proven to be the most influential parameter, but with the fabric also playing a role. It is important to highlight that two sources of error combine in the MSDD approach when predicting the thermal conductivity at any time step after the first. One is the estimation of the thermal conductivity tensors from the current state of porosity and fabric, which was demonstrated to be highly accurate in Fig. 9. The other is the prediction of the evolution of porosity and fabric up to the current state. Regardless of these error sources, the results exhibit strong agreement. With respect to the initial values in Fig. 9, the final conductivity variations are slightly underestimated by the MSDD solution in the analysis cases H and C, being more pronounced in the xx components of case C. In case HC, the effect of the global mass flux is reflected in higher conductivities near the cold wall in the DEM model, especially for the xx components.

The temperature evolution in the granular material is a direct consequence of its effective thermal conductivity. The graph in Fig. 17 compares the temperature evolution at the center (point P2) of the DEM and FVM models for all analysis cases, where the shadow lines represent the MSDD solutions with no thermal expansion shown in Fig. 11. Clearly, the proposed methodology is able to capture the thermal expansion effects with great accuracy. In particular, maximum errors of 5.3%, 2.8%, and 1.3%, relative to the maximum temperature range of each problem (50 K in cases H and C, and 100 K in case HC), were achieved for cases H, C, and HC, respectively. The thermal expansion effects lead to an acceleration of the temperature evolution pace from case H* to H, and a deceleration from case C* to C. This is

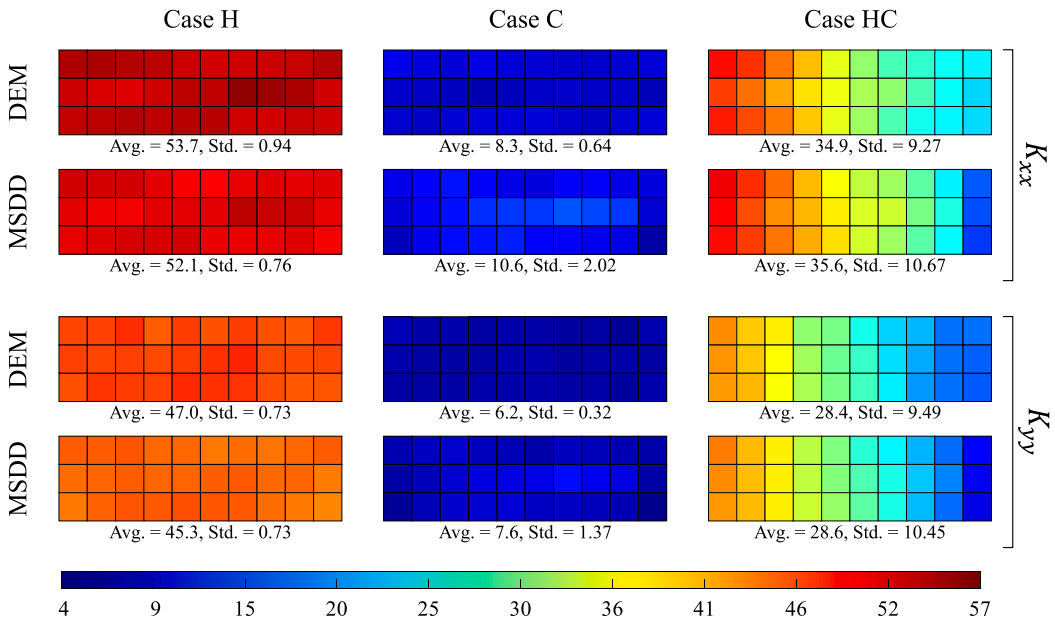

Fig. 16. Comparisons of the final values of the thermal conductivity tensor components. The average (Avg) and standard deviation (Std) of the sub-region values are indicated. All units are in W/(m·K).

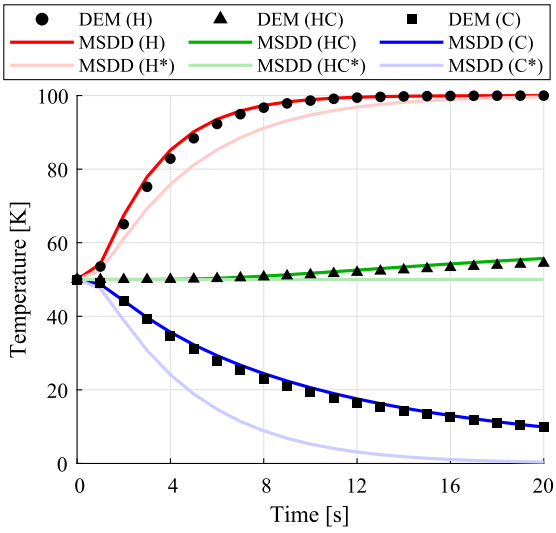

Fig. 17. Temperature evolution at the central point (P2): all analysis cases.

consistent with the evolution pace of microstructural properties seen in Fig. 12 and is caused by the change in coordination number and contact areas in each case. The small temperature rise in case HC with respect to HC* results from the asymmetry of the temperature distribution in the former; as the heated side evolves faster, the middle is more affected by the temperature of that side.

The analysis cases with an imposed temperature gradient (HC and HC*) are analyzed in more detail in Fig. 18 through the temperature evolution at points P1, P2, and P3. All results obtained with the MSDD approach are accurate, except at point P3 of case HC. The maximum errors, relative to the maximum temperature range of this case (100 k), are 2.2%, 1.3%, and 6.5% for points P1, P2, and P3, respectively. The discrepancy of the latter is a consequence of the lower thermal conductivity observed in the xx direction of the MSDD solution in Fig. 16, which, in turn, might be related to the global mass flux that is not modeled by the proposed methodology.

Finally, the stresses obtained with the two methods are compared in Fig. 19, which shows color maps of the xx and yy components of the Cauchy stress tensor at the end of each analysis case. The MSDD results are accurate in most situations. However, significant discrepancies are observed in the xx components of case HC and, more pronouncedly, in the yy components of case H. For the xx components of case HC, the MSDD solution provides higher values across the domain, except near the cold wall, where the values are lower. Again, we attribute this to the global mass flux, whose general effect is to smooth the porosity, and thus conductivity and stress, values throughout the DEM model.

The time evolution of stresses is addressed through the pressure on the walls caused by the particles. The wall pressure is computed as the mean effective stress (Eq. (11)) averaged within the domain. The results are provided in the graph of Fig. 20. Maximum errors of 9.6%, 10.9%, and 3.0%, relative to the reference stress range of each problem (3.2 kPa in case H, 2.2 kPa in case C, and 3.8 kPa in case HC), were achieved for cases H, C, and HC, respectively.

As with thermal conduction, stress prediction in the MSDD approach also involves the combination of an error related to its estimation from the current porosity and fabric with another concerning the evolution of these properties. The first error could be assessed in Fig. 10, where good accuracy was achieved, although with a slightly greater error than conductivity. On the other hand, the microstructure evolution error is expected to have more impact on the stresses due to the greater influence of the fabric on stress than on conductivity, as seen in Table 3. Since the prediction of fabric evolution had the worse training performance, it might explain the overall lower accuracy of the stress results in the MSDD solution when compared to thermal conductivity and temperature. However, we still regard these results as satisfactorily precise, especially considering that the stress is a by-product of the solution and that the simulation time to obtain these outcomes was drastically reduced.

3.2.4. Convergence analysis

The time step size can affect the MSDD solution in different ways. On the one hand, there are the discretization errors inherent to time integration strategies. In this work, we employ a first-order implicit temporal discretization to solve the heat diffusion equation with FVM at the macroscale, while a first-order explicit Gauss–Seidel scheme is used to couple the macroscale and microscale solutions, as summarized in

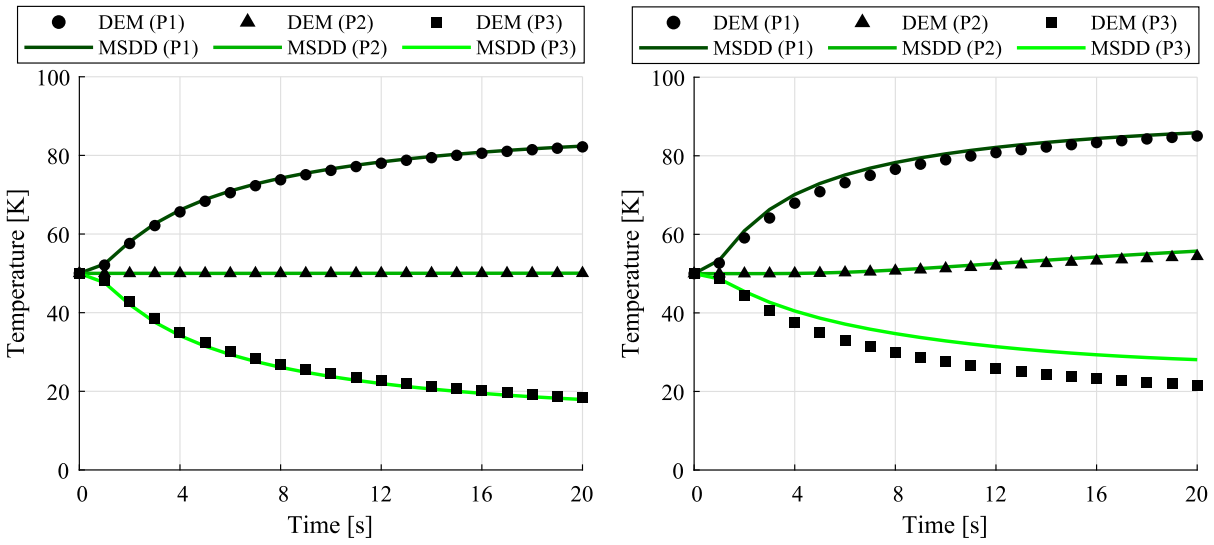

(a) Without thermal expansion (analysis case HC*). (b) With thermal expansion (analysis case HC).

Fig. 18. Temperature evolution at points P1, P2, and P3: analysis cases with imposed temperature gradient.

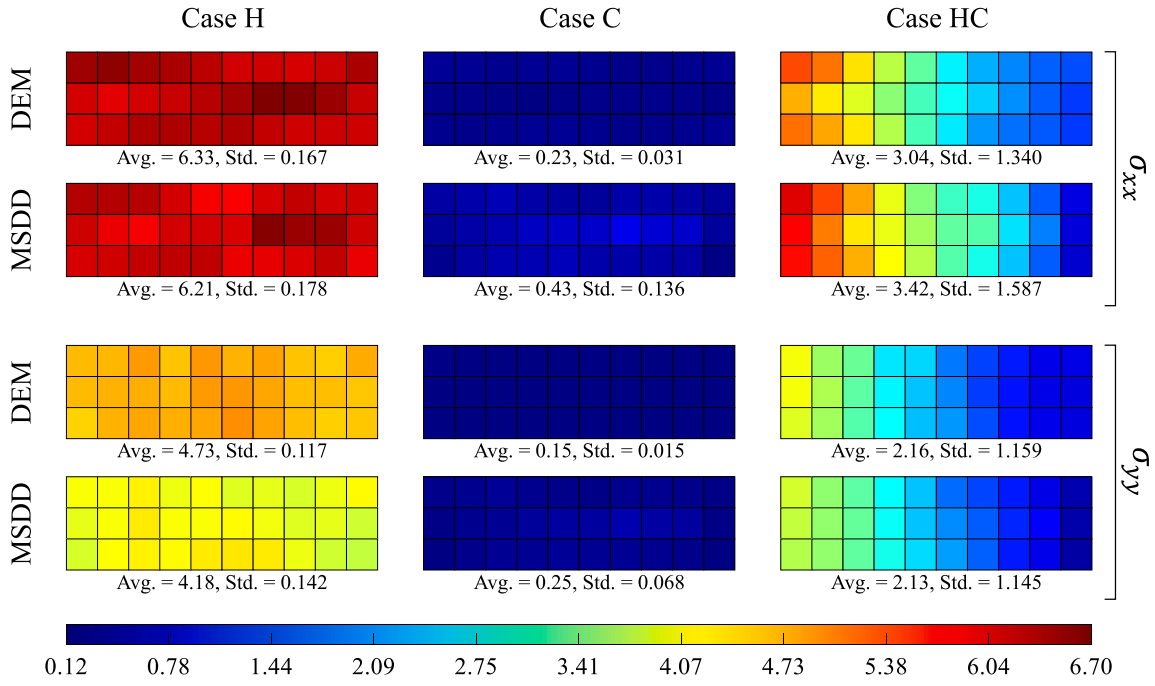

Fig. 19. Comparisons of the final values of the Cauchy stress tensor components. The average (Avg) and standard deviation (Std) of the sub-region values are indicated. All units are in kPa.

Algorithm 1. On the other hand, the time step size may also impact the ANN predictions that feed the continuous method. The reason is that the evolution of the local microstructure is computed incrementally by supplying the surrogate model with the thermal strain of each FVM cell, which is calculated in this work from the cell's temperature increment over a time step. Therefore, modifying the time step size alters the regions of the ANN prediction surfaces consulted by the online solver, potentially accessing areas with different training quality. Due to these reasons, it is important to ensure that the MSDD results converge consistently when reducing the time step size. We recall that the time step size employed for the continuum-based simulations throughout this work was 10^{-3} s.

For simplicity, only the analysis case H is presented to demonstrate the convergence behavior of the MSDD solution. The average temperature of the FVM model is taken as the representative result to evaluate convergence, given that temperature is the primary variable influencing all others. The solution with a time step size of $\Delta t = 10^{-4}$ s is considered the reference solution in this analysis. The root mean squared error (RMSE) of solutions with different step sizes is computed relative to the reference curve, and the results are shown in the log–log error convergence plot of Fig. 21. This graph reveals a power-law relationship between RMSE and time step size, which can be described by the expression $\text{RMSE} = 2.205\Delta t^{1.141}$. This indicates that the error decreases consistently with decreasing step size, presenting a slightly above-linear convergence order of 1.14. If faster convergence is desired, a higher-order scheme could be employed to couple both scales in the MSDD approach, such as the Strang splitting (Strang, 1968), along with second-order schemes for the FVM solution.

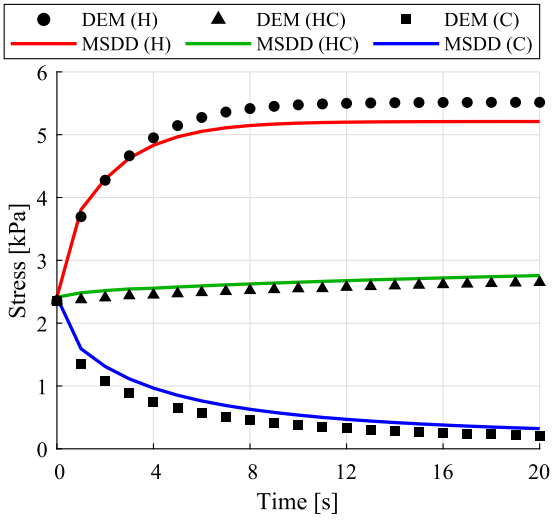

Fig. 20. Wall pressure evolution: analysis cases with thermal expansion.

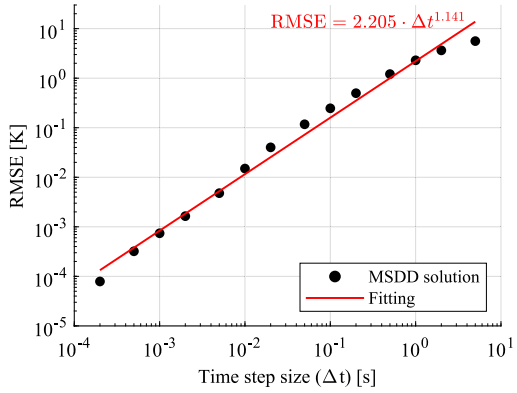

Fig. 21. Log–log error convergence plot for the FVM time step size in the MSDD solution: average temperature of analysis case H.

3.3. Limitations discussion

The limitations and sources of error identified throughout this investigation are recalled and briefly discussed. Firstly, as thoroughly assessed in our previous work (Rangel et al., 2024), the representativeness of the microscale via RVEs is limited. This is because RVEs with a sufficient number of particles can offer a good representation of a granular medium, but only up to a certain level of accuracy. Fitting errors of the ANN are also unavoidable and originate from the influence of marginally relevant parameters that are not considered as inputs of the surrogate model. In the present context, they affect the prediction of thermal conductivity and stress tensors from the current microstructure, as well as the evolution of the microstructural properties.

Additionally, in cases where a strong porosity gradient develops, a global mass flux arises. Since the RVEs are mass-conserving, the macroscale variations of porosity and fabric due to the mass flow cannot be modeled in the proposed approach. Therefore, it introduces an error that may be significant in problems where the macroscale material motion modifies sensibly the local microstructure of the granular medium. Notably, similar issues also occur in multiscale approaches using RVEs with periodic boundary conditions. The appropriate modeling of this effect in a hierarchical continuum-discrete framework could be possibly done at the macroscale level by solving a mass transport problem whose diffusion coefficient depends on certain granular material parameters. Finally, as a simplifying assumption, we neglected the off-diagonal components from the tensorial variables, which might have a minor impact due to their relatively small values.

4. Conclusions and future developments

In the present study, we proposed a novel multiscale data-driven (MSDD) methodology for simulating heat conduction in granular media considering thermal expansion. The macroscale is handled using a continuous model based on the Finite Volume Method (FVM), while the microscale is simulated with the Discrete Element Method (DEM) in Representative Volume Elements (RVEs). The RVEs are simulated offline, without needing a thermal analysis, and the results are homogenized to create a database that is used to train a surrogate model implemented as an Artificial Neural Network (ANN). The main achievements of this study are the following:

- We implemented a compact ANN with relatively few inputs related to the microstructure, demonstrating that these are optimal for predicting complex features of the microscale behavior.
- We made the inputs and outputs dimensionless to allow the surrogate model to be used for other materials with the same DEM modeling characteristics and assumptions.
- Through a broad input hyper-space, we established an extended region of valid input values to avoid extrapolations of the ANN predictions, thus ensuring reliable outputs in a given problem.
- Without any online DEM simulation, we efficiently modeled the local evolution of temperature and relevant microstructural properties, such as porosity, fabric, conductivity, and stress.
- The simulation time of the MSDD approach was shown to be drastically shorter than the high-fidelity DEM solution, while still achieving reasonably accurate results.

For future developments, we recommend exploring the effectiveness of the methodology by relaxing some assumptions. In particular, by addressing three-dimensional problems, tackling the use of different particle shapes, and generalizing the microscale database to different functions of particle size distribution or to different heat transfer models. Moreover, an important contribution is the modeling of the global mass flux effects in such a multiscale framework. Furthermore, a potential extension of the methodology is to incorporate the mechanical behavior of the material by predicting the stress–strain relationships of a moving microscale through RVE deformation analyses performed offline. Finally, since the creation of microscale databases is a time-consuming task and they can be reused in similar applications, we believe that sharing processed data for different materials, DEM models, and ranges of input parameters is a good practice. The database used in this study can be found as supplementary material of the article.

CRediT authorship contribution statement

Rafael L. Rangel: Writing – original draft, Validation, Software, Methodology, Investigation, Formal analysis, Conceptualization. **Alessandro Franci:** Writing – review & editing, Supervision, Resources, Project administration, Methodology, Investigation, Funding acquisition, Conceptualization. **Eugenio Oñate:** Writing – review & editing, Supervision, Project administration, Funding acquisition, Conceptualization. **Juan M. Gimenez:** Writing – review & editing, Supervision, Software, Project administration, Methodology, Investigation, Funding acquisition, Conceptualization.

Declaration of competing interest

The authors declare that they have no known competing financial interests or personal relationships that could have appeared to influence the work reported in this paper.

Data availability

Data will be made available on request.

Acknowledgments

The authors acknowledge the support from MCIN/AEI and FEDER *Una manera de hacer Europa* for funding this work via project PID2021-122676NB-I00.

Appendix A. Supplementary data

Supplementary material related to this article can be found online at https://doi.org/10.1016/j.compgeo.2024.106789.

References

Arabzadeh, A., Guler, M., 2019. Thermal fatigue behavior of asphalt concrete: A laboratory-based investigation approach. Int. J. Fatigue 121, 229–236.
Bonamy, D., Laurent, L., Claudin, P., Bouchaud, J.-P., Daviaud, F., 2000. Electrical conductance of a 2D packing of metallic beads under thermal perturbation. Europhys. Lett. 51 (6), 614.
Campbell, C.S., 2006. Granular material flows–an overview. Powder Technol. 162 (3), 208–229.
Chayjan, R., Montazer, G., Hashjin, T., Khoshtaghaza, M., Ghobadian, B., 2007. Prediction of pistachio thermal conductivity using artificial neural network approach. Int. J. Agricul. Biol. 9 (6), 816–820.
Chen, K., Cole, J., Conger, C., Draskovic, J., Lohr, M., Klein, K., Scheidemantel, T., Schiffer, P., 2006. Packing grains by thermal cycling. Nature 442 (7100), 257.
Chen, T., Fei, W., Narsilio, G., 2024. Effective thermal conductivity of granular soils: a review of influencing factors and prediction models towards an investigation framework through multiscale characters. Can. Geotech. J.
Chen, J., Zhang, L., Du, Y., Wang, H., Dan, H., 2021. Three-dimensional microstructure based model for evaluating the coefficient of thermal expansion and contraction of asphalt concrete. Constr. Build. Mater. 284, 122764.
Christoffersen, J., Mehrabadi, M.M., Nemat-Nasser, S., 1981. A micromechanical description of granular material behavior. J. Appl. Mech. 48, 339–344.
Coulibaly, J.B., Shah, M., Rotta Loria, A.F., 2020. Thermal cycling effects on the structure and physical properties of granular materials. Granul. Matter 22 (4), 80.
Cundall, P.A., Strack, O.D., 1979. A discrete numerical model for granular assemblies. Geotechnique 29 (1), 47–65.
Dadvand, P., Rossi, R., Oñate, E., 2010. An object-oriented environment for developing finite element codes for multi-disciplinary applications. Arch. Comput. Methods Eng. 17, 253–297.
Desu, R.K., Peeketi, A.R., Annabattula, R.K., 2019. Artificial neural network-based prediction of effective thermal conductivity of a granular bed in a gaseous environment. Comput. Part. Mech. 6, 503–514.
Fayala, F., Alibi, H., Benltoufa, S., Jemni, A., 2008. Neural network for predicting thermal conductivity of knit materials. J. Eng. Fib. Fabr. 3 (4), 155892500800300407.
Fei, W., Narsilio, G.A., Disfani, M.M., 2021. Predicting effective thermal conductivity in sands using an artificial neural network with multiscale microstructural parameters. Int. J. Heat Mass Transfer 170, 120997.
Gan, Y., Kamlah, M., 2007. Identification of material parameters of a thermo-mechanical model for pebble beds in fusion blankets. Fusion Eng. Des. 82 (2), 189–206.
Gimenez, J.M., Idelsohn, S.R., Oñate, E., Löhner, R., 2021. A multiscale approach for the numerical simulation of turbulent flows with droplets. Arch. Comput. Methods Eng. 28 (6), 4185–4204.
Go, G.-H., Lee, S.-R., Kim, Y.-S., 2016. A reliable model to predict thermal conductivity of unsaturated weathered granite soils. Int. Commun. Heat Mass Transfer 74, 82–90.
Goutorbe, B., Lucazeau, F., Bonneville, A., 2006. Using neural networks to predict thermal conductivity from geophysical well logs. Geophys. J. Int. 166 (1), 115–125.
Grabarczyk, M., Furmański, P., 2013. Predicting the effective thermal conductivity of dry granular media using artificial neural networks. J. Power Technol. 93 (2).
Guo, N., Yang, Z., Yuan, W., Zhao, J., 2021. A coupled SPFEM/DEM approach for multiscale modeling of large-deformation geomechanical problems. Int. J. Numer. Anal. Methods Geomech. 45 (5), 648–667.
Guo, N., Zhao, J., 2014. A coupled FEM/DEM approach for hierarchical multiscale modelling of granular media. Internat. J. Numer. Methods Engrg. 99 (11), 789–818.
Herrmann, H., Luding, S., 1998. Modeling granular media on the computer. Contin. Mech. Thermodyn. 10, 189–231.
Idelsohn, S.R., Gimenez, J.M., Larreteguy, A.E., Nigro, N.M., Sívori, F.M., Oñate, E., 2024. The P-DNS method for turbulent fluid flows: an overview. Arch. Comput. Methods Eng. 31 (2), 973–1021.
Idelsohn, S.R., Oñate, E., Pin, F.D., 2004. The particle finite element method: a powerful tool to solve incompressible flows with free-surfaces and breaking waves. Int. J. Numer. Methods Eng. 61 (7), 964–989.
Iliev, P.S., Giacomazzi, E., Wittel, F.K., Mendoza, M., Haselbacher, A., Herrmann, H.J., 2019. Behavior of confined granular beds under cyclic thermal loading. Granul. Matter 21, 1–7.
Ismail, K.A., Henrıquez, J., 2002. Numerical and experimental study of spherical capsules packed bed latent heat storage system. Appl. Therm. Eng. 22 (15), 1705–1716.
Kisuka, F., Rangel, R.L., Hare, C., Vivacqua, V., Wu, C.-Y., 2023. Experimental investigation of heat generation during the mixing of granular materials using an overhead stirrer. AIChE J. 69 (12), e18219.
Kruth, J.-P., Wang, X., Laoui, T., Froyen, L., 2003. Lasers and materials in selective laser sintering. Assem. Autom. 23 (4), 357–371.
Li, B., Ju, F., Xiao, M., Ning, P., 2019. Mechanical stability of granite as thermal energy storage material: An experimental investigation. Eng. Fract. Mech. 211, 61–69.
Li, K.-Q., Liu, Y., Kang, Q., 2022. Estimating the thermal conductivity of soils using six machine learning algorithms. Int. Commun. Heat Mass Transfer 136, 106139.
Liang, W., Zhao, J., 2019. Multiscale modeling of large deformation in geomechanics. Int. J. Numer. Anal. Methods Geomech. 43 (5), 1080–1114.
Liang, W., Zhao, S., Wu, H., Zhao, J., 2021. Bearing capacity and failure of footing on anisotropic soil: A multiscale perspective. Comput. Geotech. 137, 104279.
Liu, C.-h., 1994. Spatial patterns of sound propagation in sand. Phys. Rev. B 50 (2), 782–794.
Liu, C.-H., Nagel, S.R., 1994. Sound and vibration in granular materials. J. Phys.: Condens. Matter. 6 (23A), A433.
Liu, Y., Sun, W., Yuan, Z., Fish, J., 2016. A nonlocal multiscale discrete-continuum model for predicting mechanical behavior of granular materials. Internat. J. Numer. Methods Engrg. 106 (2), 129–160.
Liu, K., Xu, P., Wang, F., Jin, C., Liu, Q., Pang, H., Xie, H., 2021. The accumulated stress damage and residual life prediction of unreinforced concrete pavement with electric heating pipes. Constr. Build. Mater. 278, 122258.
Ma, G., Mei, J., Gao, K., Zhao, J., Zhou, W., Wang, D., 2022. Machine learning bridges microslips and slip avalanches of sheared granular gouges. Earth Planet. Sci. Lett. 579, 117366.
Miehe, C., Dettmar, J., 2004. A framework for micro–macro transitions in periodic particle aggregates of granular materials. Comput. Methods Appl. Mech. Engrg. 193 (3–5), 225–256.
Miehe, C., Dettmar, J., Zäh, D., 2010. Homogenization and two-scale simulations of granular materials for different microstructural constraints. Internat. J. Numer. Methods Engrg. 83 (8–9), 1206–1236.
Nguyen, T.K., Combe, G., Caillerie, D., Desrues, J., 2014. FEM× DEM modelling of cohesive granular materials: numerical homogenisation and multi-scale simulations. Acta Geophys. 62, 1109–1126.
Oda, M., 1982. Fabric tensor for discontinuous geological materials. Soils Found. 22 (4), 96–108.
Peeketi, A.R., Desu, R.K., Kumbhar, P., Annabattula, R.K., 2019. Thermal analysis of large granular assemblies using a hierarchical approach coupling the macro-scale finite element method and micro-scale discrete element method through artificial neural networks. Comput. Part. Mech. 6, 811–822.
Qu, T., Guan, S., Feng, Y., Ma, G., Zhou, W., Zhao, J., 2023. Deep active learning for constitutive modelling of granular materials: From representative volume elements to implicit finite element modelling. Int. J. Plast. 164, 103576.
Rangel, R.L., Gimenez, J.M., Oñate, E., Franci, A., 2024. A continuum–discrete multiscale methodology using machine learning for thermal analysis of granular media. Comput. Geotech. 168, 106118.
Rangel, R.L., Kisuka, F., Hare, C., Vivacqua, V., Franci, A., Oñate, E., Wu, C.-Y., 2023. Experimental investigation of heat generation during granular flow in a rotating drum using infrared thermography. Powder Technol. 426, 118619.
Reimann, J., Boccaccini, L., Enoeda, M., Ying, A., 2002. Thermomechanics of solid breeder and Be pebble bed materials. Fusion Eng. Des. 61, 319–331.
Reimann, J., Hermsmeyer, S., 2002. Thermal conductivity of compressed ceramic breeder pebble beds. Fusion Eng. Des. 61, 345–351.
Rizvi, Z.H., Zaidi, H.H., Akhtar, S.J., Sattari, A.S., Wuttke, F., 2020. Soft and hard computation methods for estimation of the effective thermal conductivity of sands. Heat Mass Transf. 56, 1947–1959.
Sablani, S.S., Baik, O.-D., Marcotte, M., 2002. Neural networks for predicting thermal conductivity of bakery products. J. Food Eng. 52 (3), 299–304.
Sassine, N., Donzé, F.-V., Harthong, B., Bruch, A., 2018. Thermal stress numerical study in granular packed bed storage tank. Granul. Matter 20, 1–15.
Singh, T., Sinha, S., Singh, V., 2007. Prediction of thermal conductivity of rock through physico-mechanical properties. Build. Environ. 42 (1), 146–155.
Strang, G., 1968. On the construction and comparison of difference schemes. SIAM J. Numer. Anal. 5 (3), 506–517.
Sulsky, D., Chen, Z., Schreyer, H.L., 1994. A particle method for history-dependent materials. Comput. Methods Appl. Mech. Engrg. 118 (1–2), 179–196.
Vargas, W.L., McCarthy, J.J., 2007. Thermal expansion effects and heat conduction in granular materials. Phys. Rev. E 76 (4), 041301.
Versteeg, H.K., Malalasekera, W., 2007. An Introduction to Computational Fluid Dynamics: The Finite Volume Method. Pearson education.

Vlahinić, I., Andò, E., Viggiani, G., Andrade, J.E., 2014. Towards a more accurate characterization of granular media: extracting quantitative descriptors from tomographic images. Granul. Matter 16 (1), 9–21.

Wang, M., Feng, Y., Guan, S., Qu, T., 2024. Multi-layer perceptron-based data-driven multiscale modelling of granular materials with a novel Frobenius norm-based internal variable. J. Rock Mech. Geotechn. Eng. 16 (6), 2198–2218.

Wang, K., Sun, W., 2018. A multiscale multi-permeability poroplasticity model linked by recursive homogenizations and deep learning. Comput. Methods Appl. Mech. Engrg. 334, 337–380.

Wang, K., Sun, W., 2019a. Meta-modeling game for deriving theory-consistent, microstructure-based traction–separation laws via deep reinforcement learning. Comput. Methods Appl. Mech. Engrg. 346, 216–241.

Wang, K., Sun, W., 2019b. An updated Lagrangian LBM–DEM–FEM coupling model for dual-permeability fissured porous media with embedded discontinuities. Comput. Methods Appl. Mech. Engrg. 344, 276–305.

Wei, H., Zhao, S., Rong, Q., Bao, H., 2018. Predicting the effective thermal conductivities of composite materials and porous media by machine learning methods. Int. J. Heat Mass Transfer 127, 908–916.

Weller, H.G., Tabor, G., Jasak, H., Fureby, C., 1998. A tensorial approach to computational continuum mechanics using object-oriented techniques. Comput. Phys. 12 (6), 620–631.

Wiebicke, M., Andò, E., Viggiani, G., Herle, I., 2020. Measuring the evolution of contact fabric in shear bands with X-ray tomography. Acta Geotech. 15 (1), 79–93.

Yang, Z., Li, X., Yang, J., 2008. Quantifying and modelling fabric anisotropy of granular soils. Géotechnique 58 (4), 237–248.

Yin, H., 2015. Full-scale test of thermally induced reflective cracking in airport pavements. Road Mater. Pavem. Des. 16 (1), 119–132.

Ying, A., Reimann, J., Boccaccini, L., Enoeda, M., Kamlah, M., Knitter, R., Gan, Y., van der Laan, J.G., Magielsen, L., Di Maio, P., et al., 2012. Status of ceramic breeder pebble bed thermo-mechanics R&D and impact on breeder material mechanical strength. Fusion Eng. Des. 87 (7–8), 1130–1137.

Yu, J., Zhao, J., Liang, W., Zhao, S., 2024. Multiscale modeling of coupled thermo-hydro-mechanical behavior in ice-bonded granular media subject to freeze-thaw cycles. Comput. Geotech. 171, 106349.

Zhang, N., Zou, H., Zhang, L., Puppala, A.J., Liu, S., Cai, G., 2020. A unified soil thermal conductivity model based on artificial neural network. Int. J. Therm. Sci. 155, 106414.

Zhao, S., Zhao, J., Lai, Y., 2020. Multiscale modeling of thermo-mechanical responses of granular materials: A hierarchical continuum–discrete coupling approach. Comput. Methods Appl. Mech. Engrg. 367, 113100.

Zhao, S., Zhao, J., Liang, W., Niu, F., 2022. Multiscale modeling of coupled thermo-mechanical behavior of granular media in large deformation and flow. Comput. Geotech. 149, 104855.

Zienkiewicz, O.C., Taylor, R.L., Zhu, J.Z., 2005. The Finite Element Method: Its Basis and Fundamentals. Elsevier.